Evolution of soot maturity in a laminar diffusion CH 4 /air flame using the two-separated pulses LII technique

G Guy, Christopher Betrancourt, Benedetta Franzelli

Evolution of soot maturity in a laminar diffusion CH_4/air flame using the two-separated pulses LII technique

G. Guy*, C. Betrancourt, and B. Franzelli

Laboratoire EM2C, CNRS, CentraleSupélec, Université Paris-Saclay, 91190 Gif-sur-Yvette, France.

Abstract

A new experimental technique is presented to measure the soot particle absorption function and the gas temperature. The approach is based only on LII and requires measuring soot particles' peak temperature at two different laser fluences. A theoretical investigation of the technique indicates the necessity to work at low fluences with two fluence values as spread as possible. Also, it shows that the underestimation of the absorption function grows with decreasing particle size. The technique has then been applied to a weakly sooting methane/air laminar diffusion flame. A coherent estimation of the absorption function is found, proving the approach's feasibility.

Introduction

Efforts are made to reduce soot emissions due to their harmful impact on health but also on the environment through radiative forcing. To that end, it is essential to better characterize the particle properties and understand their spatial and temporal evolution during their production in the flame.

Among the particle's characteristics, the absorption function $E(m_\lambda)$ is an optical property characterizing the absorption/emission of soot particles. Its value contains information on the soot particles' maturity [1, 2]. Also, knowledge of $E(m_\lambda)$ is required for the computation of soot volume fraction with some optical techniques [3, 4]. Thus, determining the evolution of $E(m_\lambda)$ would improve the estimation of soot volume fraction and provide information on the soot maturity level. Among the multiple techniques existing for estimating $E(m_\lambda)$, the most popular may be the one presented in [5], which has been applied in several works [6–9]. More recently, Yon et al. [10] presented a technique allowing to map $E(m_\lambda)$ in laminar flames. The technique is based on line-of-sight attenuation and emission measurements.

The present work describes a new approach that estimates $E(m_\lambda)$ and T_0: the two-separated pulses LII (SP-LII) technique. The main advantage of this technique is that it is based only on one optical diagnostic, i.e. on Laser Induced Incandescence (LII). The SP-LII technique is first presented. Then the experimental setup used for the testing of the technique is described. The results of an a priori analysis of the technique are given before the experimental results.

Methodology

The LII technique uses a nanosecond pulsed laser beam to heat soot particles to high temperatures. In flames, LII allows studying a specific group of soot particles as the laser-heated soot particles radiate more than the non-laser-heated ones. The collection of the soot particles' incandescence signal brings information on these soot particles.

The Separated-Pulses LII technique

The SP-LII technique computes the absorption function $E(m_\lambda)$ and the gas temperature T_0 from the measurements of the laser-heated soot particles' peak temperature at two different laser fluences. Its theoretical derivation is based on solving the energy conservation equation during the laser energy absorption phase (neglecting the thermal losses) applied to a spherical non-aggregated soot particle of diameter d_{pp}. The energy conservation equation for the internal energy U is:

$$\frac{dU}{dt} = \dot{Q}_{abs} - \dot{Q}_{cond} - \dot{Q}_{rad} - \dot{Q}_{sub}. \tag{1}$$

where $\dot{Q}_{cond}$, $\dot{Q}_{rad}$ and $\dot{Q}_{sub}$ are respectively the laser absorption power $\dot{Q}_{abs}$, and the conduction, radiation and sublimation thermal losses.

The importance of the absorption term compared to the loss terms allows to neglect all the loss terms during the laser absorption phase, providing that the laser's fluence is not important enough to induce substantial sublimation. Then, with the assumption of a spherical non-aggregated soot particle of diameter d_{pp}, and an absorption described by the Rayleigh approximation, Eq. (1) reduces to:

$$\frac{\pi d_{pp}^3}{6}\rho c\frac{dT_p}{dt} = \frac{\pi^2 d_{pp}^3 E(m_{\lambda_l})}{\lambda_l}\cdot Q_l(t), \tag{2}$$

where T_p, ρ, c and $E(m_\lambda)$ are respectively the soot particle's temperature, density, specific heat and absorption function at the laser wavelength λ_l, and t is the time. $Q_l(t)$ is the instantaneous surface power of the laser pulse, it verifies: $\int_{t_0}^{t_0+\Delta t_{pulse}} \dot{Q}_{laser}(t)dt = F$, F being the laser fluence, t_0 the beginning of the laser pulse and Δt_{pulse} its duration. By integrating Eq. (2) over the laser pulse's duration, Eq. (3) is obtained:

$$E(m_{\lambda_l}) = \rho c\frac{\lambda_l}{6\pi}\frac{T_M - T_0}{F}, \tag{3}$$

where the product ρc has been assumed constant between temperature $T_0 = T_p(t_0)$ and the maximum parti-

*Corresponding author: geoffrey.guy@centralesupelec.fr

cle's temperature, i.e. the peak temperature T_M.
For a given fluence F_i, the particle will reach a peak temperature T_{Mi}. Then, by rearranging Eq. (3) for two different laser fluences F_1 and F_2, it is possible to infer $E(m_\lambda)$ and T_0 once the temperatures T_{M1} and T_{M2} are measured by:

$$E(m_{\lambda_l}) = \frac{\lambda_l \rho c}{6\pi} \frac{T_{M_2} - T_{M_1}}{F_2 - F_1}, \tag{4}$$

$$T_0 = \frac{F_2 T_{M_1} - F_1 T_{M_2}}{F_2 - F_1}. \tag{5}$$

Eq. (4) gives the soot absorption function at the laser wavelength $E(m_{\lambda_l})$ that is noted $E(m_\lambda)$ in the following. For ρc, $4.3{\cdot}10^6$ J.K^{-1}.m^{-3} is assumed. Equation (5) gives the initial soot temperature, which is assumed to be equal to the local gas temperature. These equations are exact for spherical particles with negligible thermal losses occurring during the laser absorption phase. To compute $E(m_\lambda)$ and T_0, the peak particle temperature is measured by two color LII pyrometry.

Two Color LII pyrometry (2C-LII)

The soot particles' peak temperature is computed by the widely used 2C-LII pyrometry [3, 7, 9] via:

$$T_M = \frac{hc_l}{k_B}\left(\frac{1}{\lambda_2} - \frac{1}{\lambda_1}\right) \frac{1}{\ln\left(\frac{S_{LII_{\lambda_1}}}{S_{LII_{\lambda_2}}} \frac{E(m_{\lambda_2})}{E(m_{\lambda_1})} \left(\frac{\lambda_1}{\lambda_2}\right)^6 \frac{\Delta\lambda_2}{\Delta\lambda_1} \frac{\Sigma_{\lambda_2}}{\Sigma_{\lambda_1}}\right)}, \tag{6}$$

where h and k_B are respectively, the constants of Planck and Boltzmann. c_l is the light celerity. λ_1 and λ_2 are the two central collection wavelengths of the collection system (578 and 716 nm, in this work), $\Delta\lambda_1$ and $\Delta\lambda_2$ are the widths of the collection windows. $\frac{S_{LII_{\lambda_1}}}{S_{LII_{\lambda_2}}}$ is the ratio of the maximum of the LII signals detected at wavelengths λ_1 and λ_2. $\frac{\Sigma_{\lambda_2}}{\Sigma_{\lambda_1}}$ is the ratio of calibration constants at the collection wavelengths, which depends on the collection system. The ratio $\frac{E(m_{\lambda_1})}{E(m_{\lambda_2})}$ is assumed to be unity for all soot particles. This assumption is expected to not greatly affect the results. Indeed, for mature soot particles, for $\lambda >\sim 500$ nm, $E(m_\lambda)$ is weakly dependent on wavelength [8]. For younger soot, the wavelength dependency of $E(m_\lambda)$ is stronger, but mostly in the UV region and in the early visible region. As in this work, the selected collection wavelengths are in the upper visible region and are not too spread, the difference between $E(m_{\lambda_1})$ and $E(m_{\lambda_2})$ is limited.

Auto-Compensated LII (AC-LII)

In addition to the information on $E(m_\lambda)$ and T_0, the LII signal provides access to a quantitative characterisation of the soot volume fraction f_v via AC-LII [3].

LII code

An in-house LII code [11] is used to a priori evaluate the performance of the SP-LII technique. This LII code solves Eq. (1) for monodispersed soot particles. The internal energy and absorption terms are given respectively by the terms on the left and right-hand sides of Eq. (2). The expression of the radiative loss term is the one in [12]. The model for the conduction term (in the free-molecular regime) is given by the expression found in [13]. The sublimation term is the expression of Hoffman in [14]. The reference input parameters of the LII code are gathered in Tab. 1. Thermal and mass accommodation coefficient (respectively α and β) describe the intensity of the conduction and the sublimation terms respectively. They are characterised by high uncertainties. α is set to 0.3, a value largely encountered in literature [14]. β is set to 1 (its maximum possible value) to test the SP-LII in unfavourable conditions, i.e. where sublimation rapidly becomes not negligible with increasing laser fluence.

Inputs of the LII code		
Parameter	**Unit**	**Value**
$E(m_\lambda)_{ref}$	–	0.37
$T_{0_{ref}}$	K	1860
$F_{1_{ref}}$	$J.cm^{-2}$	0.07
$F_{2_{ref}}$	$J.cm^{-2}$	0.14
$d_{p_{ref}}$	nm	26
ρ_{ref}	$kg.m^{-3}$	1950
α_{ref}	–	0.3
β_{ref}	–	1

Table 1: Reference input parameters of the LII code.

Experimental setup

The burner is a Yale diffusion co-flow burner mounted on a 3-axis translation stage. The methane is injected through the central fuel injector of ∼3.9 mm inner diameter. Flame is stabilised thanks to an air co-flow flowing through a porous surface of 4.8 mm inner diameter and 49.5 mm outer diameter surrounding the injector. Mass flow controllers impose methane and air mass flow rates to respectively 0.20 and 30 ln.min^{-1} (0°C and 1 atm). The obtained flame is a stabilised ∼4 cm laminar diffusion flame (Fig. 1).

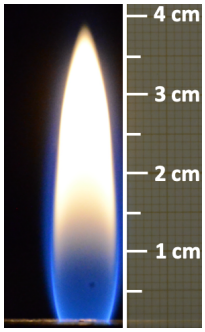

Figure 1: Image of the CH4/air flame stabilised on the Yale diffusion burner.

The experimental setup is presented in Fig. 2.

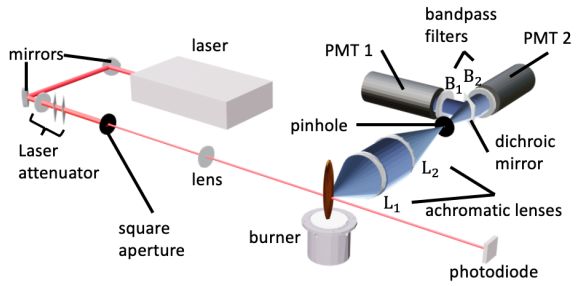

Figure 2: Scheme of the LII experimental bench.

The laser source is a Powerlite Continuum laser, operating at λ_l = 1064 nm, with a FWHM duration of ~8 ns. A laser attenuator composed of a half-wave plate and two polarisers allows varying the laser beam's fluence. A 1 mm square aperture selects the most uniform part of the laser beam, and a lens (f = 30 cm) relays the image of this aperture to form a nearly top-hat laser beam above the burner in the flame. The laser pulse's energy is measured with an energy measurer (GENTEC-EO QE25LP-S-MB-D0). The LII signal is collected at 90° from the laser beam.

The achromatic lenses L_1 and L_2 of the collection system have a focal length of respectively f_1 = 15 cm and f_2 = 20 cm. The signal is focused on a 500 μm diameter pinhole, resulting in a spatial resolution of 375 μm.

A dichroic mirror (Semrock FF605-Di02-25x36) with a cut-off wavelength of 605 nm separates the radiations according to their wavelength. Wavelengths below 605 nm go through the bandpass filter B_1, centred on 578 nm (Edmund optics 87766) before being collected by a first photomultiplier tube (PMT) (HAMAMATSU R2257). Higher wavelengths go through the bandpass filter B_2, centred on 716 nm (Edmund optics 67053) and are collected by a second PMT.

After crossing the flame, the laser beam is collected by a photodetector (DET10A2) to monitor the laser energy stability and to trigger the signal acquisition with an 8-bit Lecroy WS434 oscilloscope. The oscilloscope records the signals at 1Gs/s for 500 ns. As the flame is laminar and steady, the samples are averaged over 700 single-shots to ensure a good signal-to-noise ratio. The flame background is subtracted from the LII signal. The system is calibrated using a calibrated integrating sphere (OL-455-2) placed at the flame's location.

Results and discussion

Theoretical analysis

The LII code is used to perform simulations representative of LII experiments. The main outputs of the simulations are the soot particles' peak temperatures. To investigate the effect of neglecting losses (radiation, conduction and sublimation), simulations are done by activating one by one the loss terms in Eq. (1). Multiple values of the second pulse fluence F_2 were considered. From the obtained peak temperatures at the two laser fluences considered, $E(m_\lambda)$ and T_0 are computed with Eq. (4) and Eq. (5). The computed values are compared to their reference values, i.e. the values used as input of the LII code (see Tab. 1).

The results are represented as deviations from the reference value of $E(m_\lambda)$ and T_0 in Fig. 3. The deviations are defined as $\frac{X-X_{ref}}{X_{ref}}$ where X is either $E(m_\lambda)$ or T_0. With all loss terms deactivated in the LII code, the reference values are exactly retrieved. This points out the validity of Eq. (4) and Eq. (5). When only the radiation loss term is present, the deviations are almost null, showing that radiation losses are negligible. Adding the conduction brings a small deviation of $\approx$ 2% for $E(m_\lambda)$. With sublimation activated, no additional deviations are visible for $F_2 < 80$ mJ.cm^{-2}. However, for higher fluences, the deviation rapidly grows with F_2. The deviation for $E(m_\lambda)$ is almost twice as important as that on T_0. It has to be noted that the threshold limit of 80 mJ.cm^{-2} is probably lower than in reality as the sublimation term was set to $\beta = 1$.

Thus, radiative and conduction loss terms can be neglected without introducing high errors on the determination of $E(m_\lambda)$ and T_0. However, sublimation has to be avoided as much as possible by limiting the laser fluences. In the following, the simulations are run with all loss terms activated in the LII code.

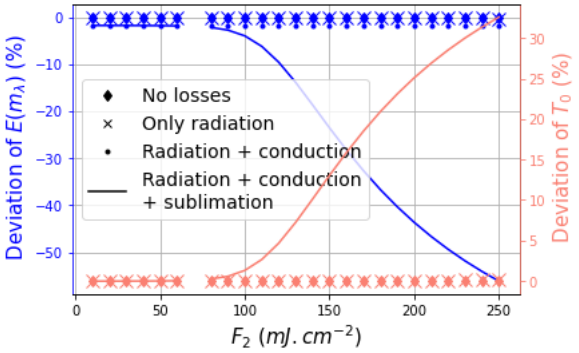

Figure 3: Deviations of $E(m_\lambda)$ (blue line) and of T_0 (pink line) from their reference values, as a function of F_2 when different loss terms are considered in Eq. (1): no losses (♢), radiation (×), radiation and conduction (•), and radiation, conduction and sublimation (solid lines).

Equations (4) and (5) are independent from the particle diameter d_{pp}. However, d_{pp} influences the loss terms. Thus, simulations are run with the reference input parameters except for d_{pp}, which is varied from 1 to 41 nm. The resulting deviations of $E(m_\lambda)$ and T_0 in Fig. 4 show that smaller particles suffer from higher deviations, especially for $E(m_\lambda)$. These larger deviations are explained by the larger surface-to-volume ratio for smaller particles, favouring conduction losses. The non-negligible deviations for the large particles are mainly explained by the value of F_{2ref} that is high enough to

induce sublimation. To conclude, the SP-LII technique tends to underestimate $E(m_\lambda)$, especially for small soot particles ($d_{pp} \sim< 10$ nm).

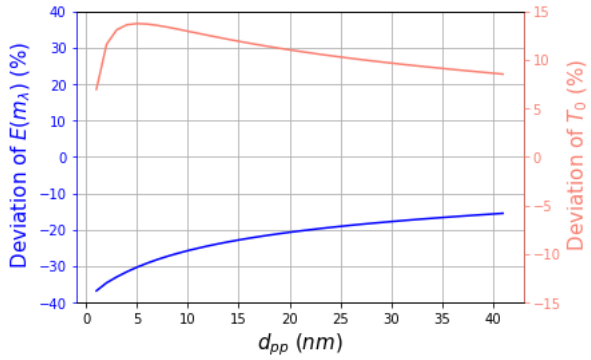

Figure 4: Deviations of $E(m_\lambda)$ (blue line) and T_0 (pink line) as a function of d_{pp} .

Finally, the experimental determination of the peak temperatures by 2C-LII is potentially subjected to errors. To evaluate the impact of such errors, the value of T_{M1} extracted from the simulation results is increased by 10% to mimic an error on its experimental estimation. Different F_2 values are considered, and T_{M2} is extracted from the simulations without introducing errors. The resulting deviations in terms of $E(m_\lambda)$ and T_0 are given in Fig. 5. This figure shows important deviations for both $E(m_\lambda)$ and T_0 with a minimum near $F_2 = 125$ mJ.cm^{-2}. For the highest values of F_2, the high deviations are explained by the non-negligible sublimation level of the soot particles. For the smallest values of F_2, the deviations skyrocket when F_2 approaches F_{1ref} as the 10% error done on T_{M1} gains importance on the numerator terms of Eqs. (4) and (5), while the denominators approach 0. In practice, to limit the errors, the laser fluences F_1 and F_2 should be selected as spread as possible considering the signal-to-noise ratio of the experiment, which determines the lower fluence limit and the sublimation threshold of the probed soot particles, which prescribes the highest fluence limit.

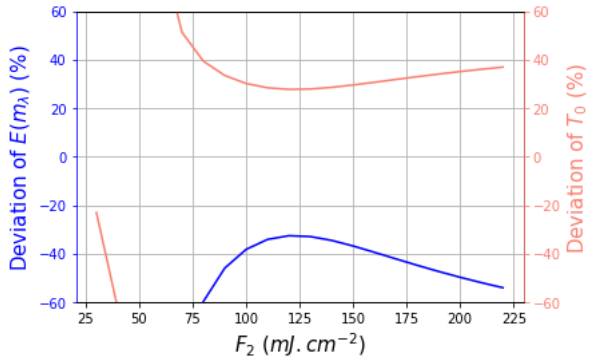

Figure 5: Deviations of $E(m_\lambda)$ (blue line) and T_0 (pink line) as a function of F_2 when T_{M1} is overestimated by 10%.

Experimental results

The SP-LII technique is applied to a laminar diffusion methane/air flame. As deduced from the previous theoretical analysis, the selection of laser fluences is crucial. Measurements of particles' peak temperature by 2C-LII pyrometry are done at multiple Heights Above the Burner (HAB) and for various laser fluences to assess the best laser fluence couple. Results are presented in Fig. 6.

The five curves show a linear behaviour between 2600 K and 4000 K. The limit of 4000 K represents the upper limit for the linear regime. Above this value, high-temperature phenomena, like sublimation, may be responsible for the observed loss of linearity and cause the measurements to fall outside the assumptions of the SP-LII technique. The lower limit of 2600 K is introduced to guarantee that the flame emission has a non-negligible weight compared to the LII emission of the probed soot particles, avoiding then erroneous peak temperature estimations. According to Eq. (3), the slope of the curves in the linear regime depends only on $E(m_\lambda)$ once ρc is set. Thus, the observed differences in slopes illustrate soot population with different $E(m_\lambda)$. It has to be noted that the soot particles for HAB$\geq$32 mm have a similar $E(m_\lambda)$ since their slope is similar, while the soot particles at HAB=29 and 30 mm have a noticeable lower slope value. This indicates a rapid evolution of $E(m_\lambda)$ with HAB on the centreline, followed by a quasi-plateau value. The blue zone identifies the fluences that allow to compute $E(m_\lambda)$ with the SP-LII technique for the soot particles from HAB=29 mm to HAB=36 mm. Thus, a couple of laser fluences F_1 and F_2 selected in this zone allows computing $E(m_\lambda)$ and T_0 from 29 to 36 mm.

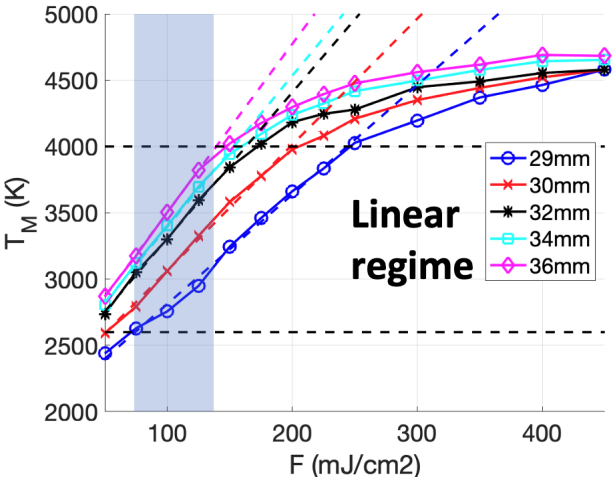

Figure 6: Particles' peak temperature as a function of laser fluence for five different HABs along the flame centerline: 29 mm (blue o), 30 mm (red x), 32 mm (black $*$), 34 mm (cyan $\square$) and 36 mm (magenta $\diamondsuit$). The horizontal dashed lines represent the temperatures limits of 2600 K and 4000 K. The oblique dashed lines represent linear regressions of the temperature curves in the linear regime. The blue zone represents the fluences compatible with the SP-LII technique for the five HABs.

Three fluences are selected to establish measurements of T_M in different flame locations along the flame's axis and for different radial positions. The selected fluences are 75, 125 and 175 mJ.cm^{-2}. The couple 75/125 mJ.cm^{-2} is adapted to the mature soot particles as the peak temperature stays below 4000 K, while 125/175 mJ.cm^{-2} is adapted to younger soot particles as the soot-heating brings sufficient signal. Estimation of $E(m_\lambda)$ and T_0 are gathered in 2D maps in Fig. 7.

On the flame's axis, $E(m_\lambda)$ increases from about 0.1 at HAB=28 mm up to 0.3 near HAB=31mm and remains constant up to the signal detection threshold at HAB=36 mm. $E(m_\lambda)$ increases rapidly with the radial position at lower HABs (23, 25, 28 mm). It stays constant and equal to ≈ 0.3 for HAB=31 and 35 mm. A smaller probe volume would be necessary to properly catch the rapid radial evolution of $E(m_\lambda)$.

These values and the tendency to increase with HAB are coherent with literature for premixed flames [6–9] although the values found in this work are slightly lower for the mature soot. Yon et al. [10] presented a 2D profile of $E(m_{\lambda=810\text{nm}})$ for an ethylene/air laminar diffusion flame stabilised on a Gülder burner. Globally, their results are consistent with the present work: they found $E(m_\lambda)$ values ranging from 0.1 to 0.4, with the highest values for $E(m_\lambda)$ at the outer part of the flame, while the lower values are found in the lower and inner regions of the flame. One significant difference with the present work is that $E(m_\lambda)$ is quasi-constant along the flame's axis before rapidly increasing to 0.4 at the flame's tip. This rapid increase is not seen in Fig. 7. At this stage, it is not possible to know if this discrepancy comes from the differences in experimental conditions or a bias in one of the experimental techniques.

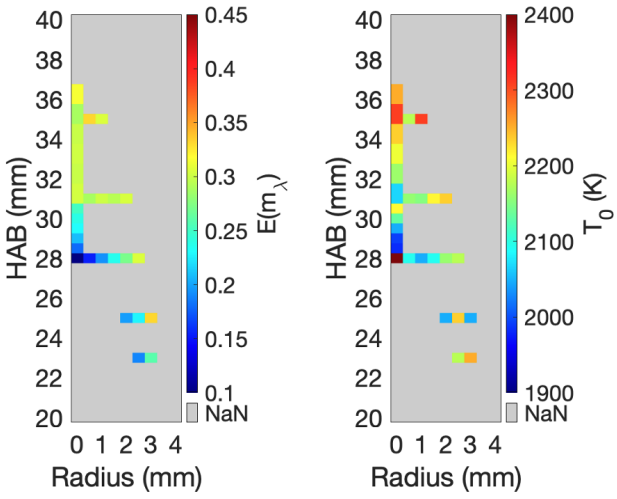

Figure 7: Left: distribution of absolute value of $E(m_\lambda)$. Right: distribution of T_0.

The second figure of Fig. 7 gives the gas temperature estimated by the SP-LII. T_0 ranges from 2000 to 2400 K, which is high for an atmospheric methane/air flame. This high estimation of T_0 may be explained by fluences high enough to start sublimation (the limit of 4000 K may be too permissive), which tends to overestimate T_0 and underestimate $E(m_\lambda)$ (Fig. 3). Also, according to Fig. 4, when sublimation is not negligible, for small particles ($\sim$ 10 nm), T_0 is further overestimated while $E(m_\lambda)$ is further underestimated. Thus, it could also explain the slightly lower values of $E(m_\lambda)$ compared to the literature. However, in this flame, it is difficult to reduce the laser fluences keeping a constant difference between them because of the signal-to-noise ratio limit.

Fig. 8 represents the soot volume fraction in the flame computed with AC-LII [3] considering the distribution of $E(m_\lambda)$ of Fig. 7 (left figure). The case of constant $E(m_\lambda)$ is also computed considering a value representative of mature soot: $E(m_\lambda) = 0.3$ (right figure). Considering a spatially uniform absorption function value (correspondent to mature soot) brings an underestimation of the soot quantity where soot particles are young with a slight shift in the location of maximum f_v to higher HABs on the flame's axis. The considered diffusion flame is weakly sooting as $f_{v\,max}$ is less than 100 ppb near HAB=31 mm before decreasing due to oxidation. The soot particles are mostly found near the flame's axis and not in the wings.

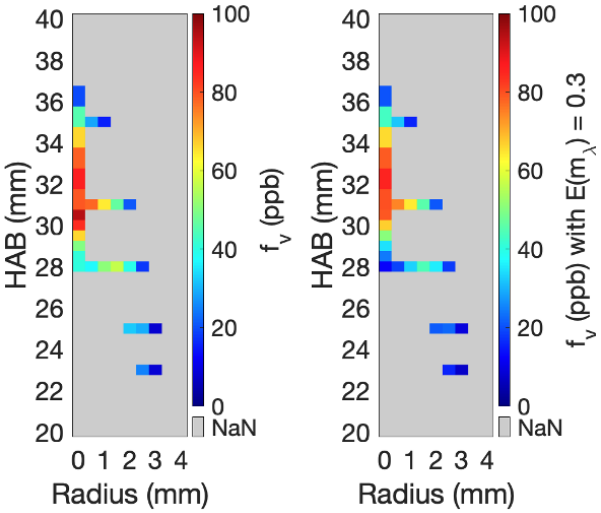

Figure 8: Left: distribution of f_v computed using the spatial evolution of $E(m_\lambda)$ of Fig. 7. Right: distribution of f_v computed considering a spatially uniform $E(m_\lambda) = 0.3$.

Conclusion

The SP-LII technique is a new experimental technique aiming to estimate the soot absorption function and gas temperature from the measurements of peak temperature of laser-heated soot particles at two different laser fluences.

An a priori analysis based on numerically synthesised LII signals shows the necessity to avoid high fluences that bring an underestimation of the absorption function. The error made on the absorption function in-

creases with decreasing primary particle diameter. Also, the laser fluences must be selected as spread as possible to reduce the effect of an error on the peak temperature estimations.

Then, the feasibility of the SP-LII was proven on a methane/air laminar diffusion flame for the first time. Curves of peak temperature as a function of laser fluences obtained at different HABs on the flame centreline were presented to discuss the selection of the couples of laser fluences. Estimation of absorption function and gas temperature at multiple axial and radial positions are gathered in 2D maps. The absorption function increases from $\sim$0.1 in the lower and inner part of the flame up to a maximum of $\sim$0.3 at the flame's outer edges. These values and trends are consistent with the literature, although the values are generally smaller than the literature. The too-high estimation of T_0 may indicate that the selected fluences are too high and induce high-temperature phenomena like phase change that should be avoided with the SP-LII technique. This would also mean that the absorption function is underestimated. Accounting for the evolution of the absorption function across the flame slightly shifts the position of the maximum soot volume fraction to lower HABs compared to the assumption of constant $E(m_\lambda)$. It also allows estimating better the soot quantity in flame regions with young soot particles.

Acknowledgments

The support of the European Research Council (ERC) under the European Union Horizon 2020 research and innovation programme (grant agreement No. 757912) is gratefully acknowledged, as well as Alberto Cuoci for the sharing of the LII code.

References

[1] F. Liu, J. Yon, A. Fuentes, P. Lobo, G. J. Smallwood, and J. C. Corbin, Review of recent literature on the light absorption properties of black carbon: Refractive index, mass absorption cross section, and absorption function, *Aerosol Science and Technology* **54**, 33 (2020).

[2] K. O. Johansson, F. El Gabaly, P. E. Schrader, M. F. Campbell, and H. A. Michelsen, Evolution of maturity levels of the particle surface and bulk during soot growth and oxidation in a flame, *Aerosol Science and Technology* **51**, 1333 (2017).

[3] D. R. Snelling, G. J. Smallwood, F. Liu, O. L. Gulder, and W. D. Bachalo, A calibration-independent laser-induced incandescence technique for soot measurement by detecting absolute light intensity, *Applied Optics* **44**, 6773 (2005).

[4] C. Betrancourt, X. Mercier, F. Liu, and P. Desgroux, Quantitative measurement of volume fraction profiles of soot of different maturities in premixed flames by extinction-calibrated laser-induced incandescence, *Applied Physics B* **125**, 16 (2019).

[5] D. R. Snelling, F. Liu, G. J. Smallwood, and O. L. Gulder, Determination of the soot absorption function and thermal accommodation coefficient using low-fluence LII in a laminar coflow ethylene diffusion flame, *Combustion and Flame* **136**, 180 (2004).

[6] S. Bejaoui, S. Batut, E. Therssen, N. Lamoureux, P. Desgroux, and F. Liu, Measurements and modeling of laser-induced incandescence of soot at different heights in a flat premixed flame, *Applied Physics B* **118**, 449 (2015).

[7] H. Bladh, J. Johnsson, N. E. Olofsson, A. Bohlin, and P. E. Bengtsson, Optical soot characterization using two-color laser-induced incandescence (2C-LII) in the soot growth region of a premixed flat flame, *Proceedings of the Combustion Institute* **33**, 641 (2011).

[8] A. V. Eremin, E. V. Gurentsov, and R. N. Kolotushkin, The change of soot refractive index function along the height of premixed ethylene/air flame and its correlation with soot structure, *Applied Physics B* **126**, 125 (2020).

[9] S. Maffi, S. De Iuliis, F. Cignoli, and G. Zizak, Investigation on thermal accommodation coefficient and soot absorption function with two-color Tire-LII technique in rich premixed flames, *Applied Physics B* **104**, 357 (2011).

[10] J. Yon, J. J. Cruz, F. Escudero, J. Morán, F. Liu, and A. Fuentes, Revealing soot maturity based on multi-wavelength absorption/emission measurements in laminar axisymmetric coflow ethylene diffusion flames, *Combustion and Flame* **227**, 147 (2021).

[11] A. L. Bodor, A. Cuoci, T. Faravelli, and B. Franzelli, A forward approach for the validation of soot sizing models using laser-induced incandescence (LII), *Applied Physics B* **126**, 49 (2020).

[12] F. Liu, M. Yang, F. Hill, D. Snelling, and G. Smallwood, Influence of polydisperse distributions of both primary particle and aggregate size on soot temperature in low-fluence LII, *Applied Physics B* **83**, 383 (2006).

[13] A. V. Filippov and D. Rosner, Energy transfer between an aerosol particle and gas at high temperature ratios in the knudsen transition regime, *International Journal of heat and mass transfer* **43**, 127 (2000).

[14] H. Michelsen, F. Liu, B. Kock, H. Bladh, A. Boiarciuc, M. Charwath, T. Dreier, R. Hadef, M. Hofmann, J. Reimann, et al., Modeling laser-induced incandescence of soot: a summary and comparison of LII models, *Applied Physics B* **87**, 503 (2007).